CCFE
CULHAM CENTRE FOR FUSION ENERGY

UK Atomic Energy Authority

UKAEA-CCFE-PR(18)2

Alexandra Cackett, Joven Lim, Chris Hardie, Peter Klups and Andy Bushby

Using spherical indentation to measure the strength of copper-chromium-zirconium

Using spherical indentation to measure the strength of copper-chromium-zirconium

Alexandra Cackett,[a, b] Joven Lim,[a] Chris Hardie,[a]
Peter Klups [a, b] and Andy Bushby[b]

[a]*CCFE, UK Atomic Energy Authority, Abingdon, Oxfordshire, OX14 3DB, UK*
[b]*Queen Mary University of London, Mile End Road, London, E1 4NS, UK*

This is a preprint of a paper submitted for publication in Journal of Nuclear Materials

Using spherical indentation to measure the strength of copper-chromium-zirconium

Alexandra Cackett[a,b], Joven Lim[a], Chris Hardie[a], Peter Klups[a,b], Andy Bushby[b]

[a] *CCFE, UK Atomic Energy Authority, Abingdon, Oxfordshire, OX14 3DB, UK*
[b] *Queen Mary University of London, Mile End Road, London, E1 4NS, UK*

alexandra.cackett@ukaea.uk

joven.lim@ukaea.uk

chris.hardie@ukaea.uk

p.klups@se13.qmul.ac.uk

a.j.bushby@qmul.ac.uk

Corresponding author: Alexandra Cackett

Keywords: Cu-Cr-Zr; ISE; spherical indentation;

Declaration of interest: none.

Abstract

Precipitation-hardened CuCrZr will be used in heat-sink components in the Iter tokomak. After irradiation it will not be possible to test the mechanical properties of CuCrZr using conventional, large-scale, techniques and methods requiring reduced sample sizes will have to be used. Spherical nano-indentation is one such method. In this work, CuCrZr has been heat-treated at different temperatures to vary the Cr precipitate size and spacing. Spherical nano-indentation using multiple tip radii was then used to produce stress-strain curves for all samples, from which values of yield pressure were calculated. It was found that there was a strong indentation size effect in yield pressure values, however at higher indentation strain the response became size-independent at tip sizes above ~10 μm. This supports the theory that at the initiation of plastic deformation the ISE is due to dislocation source activation but in later stages of it is the interaction with intrinsic material length-scales that dominates the measured mechanical strength.

Highlights:

- The hardness of CuCrZr was measured using spherical nano-indentation
- A strong indentation size effect was seen in the yield point but not at high strains
- Microstructural length-scales dominate size effect at higher indentation strain

1 Introduction

Due to its high thermal conductivity, high strength at elevated temperature, good radiation resistance, and commercial availability [1,2], copper-chromium-zirconium (CuCrZr) has for many years been used to make actively cooled plasma facing components in fusion reaction vessels [3]. This copper-based, precipitation-hardened alloy has also been selected as the heat sink material for the International Thermonuclear Experimental Reactor (ITER); the optimised chemical composition for ITER-grade CuCrZr specifies the alloying elements as being in the range 0.6-0.9 wt.% chromium and 0.07-0.15 wt.% zirconium with ≤0.15 wt.% impurities [4]. Peak strength is then achieved by aging the material at 480 °C in a vacuum furnace. When used for this purpose in a reactor the material will be irradiated with high-energy neutrons and so become active. Small-scale testing techniques will therefore be required to monitor the condition of the component as large specimen volumes pose a health and safety risk.

There are a range of small-scale experimental techniques that can be used to measure the mechanical properties of materials and investigate the mechanisms responsible for plastic deformation. Micro- and nano-pillar compression have extensively been used for this purpose [5–7], with in-situ studies providing additional information on fundamental processes such as slip step formation, and dislocation generation and movement [8,9]. Cantilever flexure is commonly used for experiments in fracture mechanics and cyclic fatigue [10–12]. Both these techniques require fabrication of miniaturised test pieces, typically carried out using a focussed ion beam (FIB), which can be expensive in terms of both time and facility costs. One method that does not require intensive sample preparation is instrumented indentation testing (IIT). This technique is now highly automated and can perform a large number of tests in a short amount of time. Also, when sample size is limited (e.g. in thin films or ion-irradiated material), nano-indentation can be used to probe the very first few tens – hundreds nm's.

IIT using a spherical indenter tip has some advantages over using pointed indenters; due to the blunt geometry, spherical indentation is initially elastic, therefore the whole range from elastic, plastic-elastic, and finally fully plastic deformation can be observed. This has made it is possible to generate indentation stress-strain curves comparable to those from traditional tensile tests. Results from

indentation tests are, however, influenced by the indentation size effect (ISE), whereby the smaller the contact area between tip and sample the stronger the material appears. The ISE has been the subject of many studies over the last two decades [16–19]. For Berkovich indentation a change in penetration depth that causes a change in measured hardness; the shallower the indent the harder the material appears. For spherical indentation, it is the tip radius that governs the size effect, with a decrease in tip radii measuring a higher hardness. Such test-piece (extrinsic) size effects are distinguished separately from the well-established size effect due to microstructural (intrinsic) length-scales, e.g. grain size or film thickness [20–22].

Initial reasoning for the ISE was hypothesised by Fleck et al. [23] who suggested that since geometrically necessary dislocations (GND's) are required for material deformation in a restricted volume, small indentations appear stronger because GND density scales with the plastic strain gradient, which is higher for smaller penetration depths. This theory was later expressed by a model by Nix and Gao [24], which showed good agreement with experimental data for Berkovich indentation in Ag and Cu. However strain gradients cannot be the cause of all extrinsic size effects; for example uniaxial micro-pillars have unconstrained geometry yet still exhibit a 'smaller is stronger' behaviour [25]. There have since been many studies exploring further plasticity mechanisms that account for test piece size effects, which show that that dislocation starvation and dislocation curvature also contribute to this phenomenon [26–28].

In this work, indentation using spherical tips with a range of radii between 2 and 90 μm has been used to probe CuCrZr samples that have been heat-treated at different temperatures. The heat-treatments have the effect of changing the dominant internal length-scale of the material, in this case the average distance between Cr precipitates, which was characterised using transmission electron microscopy (TEM). The aim of the study was to observe the impact of the ISE in combination with intrinsic size effects in order to give insights into the dominant mechanisms of dislocation plasticity in a precipitation-hardened alloy.

2 Material and methods

A piece of ITER-grade Cu-1.0%Cr-0.06%Zr (wt%) in the solution annealed state (970 °C followed by water quenching) was divided into seven blocks; one block remained as-received ('AR') and the other six were heat-treated for two hours in a vacuum furnace at the following temperatures: 400, 480, 550, 600, 650, and 700 °C. To highlight the main results in this paper, four of these have been chosen as the focus: AR, 400, 480 and 500 °C. Previous studies have already shown that chromium precipitates grow in size and the distance between them increases with higher aging temperatures [29,30], therefore the aim of the heat treatments was to generate a range of internal length-scales. For nano-indentation, small samples were cut from each of the heat-treated blocks and mechanically polished with SiC abrasive paper down to a 2.5 µm grit size. They were then electropolished in a nitric acid and methanol 1:4 mix to produce a deformation-free flat surface. This electrolyte solution was also used to twin-jet polish 3 mm discs for observation in the transmission electron microscope (TEM). Instrumented nano-indentation was performed using a Keysight G200 with spherical tips of radii 2, 8, 15, 30, and 90 µm. Tip geometry as a function of indentation depth was determined via the calibration method described by Bushby and Jennett in [31], using reference samples of fused silica, sapphire, and glassy carbon. Indentation data was collected using a load-controlled, modified Field and Swain [32] approach with 40 load partial unload cycles per indent. Arrays consisting of a grid of 4x4 locations for the four smallest indenter tips and 3x3 for the largest, due to the increased area required to accommodate adequate spacing between indents, were run for each test.

A Tescan MIRA3 FEG Scanning Electron Microscope (SEM) was used to perform electron back-scatter diffraction (EBSD). The EBSD maps were then used to make grain size measurements using Channel5 software Tango, which used elliptic fits to the grains in order to calculate the geometric mean area and diameter. To measure precipitate size and spacing, a 200 kV FEI Talos scanning transmission electron microscope (STEM) in the University of Manchester's School of Materials was used. Bright- and dark-field micrographs were taken as well as chemical maps, which were acquired using the Super X-EDS (energy dispersive spectroscopy) system with four silicon drift detectors.

Precipitate size and spacings were calculated from the EDS maps using the particle analysis plugin in Fiji [33].

3 Theory

The contact depth between sample surface and indenter tip was calculated using Hertzian contact mechanics [34]; using the assumption that the unloading curve is purely elastic, Hertzian contact of a sphere and a concave residual impression can be described by the following equation:

$$h_e = \left(\frac{9}{16}\right)^{\frac{1}{3}} \left(\frac{F}{E^*}\right)^{\frac{2}{3}} \left(\frac{1}{R} - \frac{1}{R'}\right)^{\frac{1}{3}} \qquad (1)$$

where F is the force applied, R is the tip radius, R' is the residual impression radius. E^* is the reduced modulus, defined as follows:

$$\frac{1}{E^*} = \frac{1-\upsilon_i^2}{E_i} + \frac{1-\upsilon_s^2}{E_s} \qquad (2)$$

where υ is Poisson's ratio and the subscripts i and s refers to the indenter the surface respectively. The radius of the residual impression, h_r, is calculated on a per-cycle basis by extrapolating the unload curve back to the x-axis when the data is displayed on a load-displacement plot.

The contact radius between tip and surface, a, is simply a geometric relationship:

$$a = \sqrt{2R^* h_c - h_c^2} \qquad (3)$$

Where the contact depth, h_c, is defined as

$$h_c = \frac{h_1 + h_r}{2} \qquad (4)$$

with h_1 being the indentation depth at maximum load. Indentation strain and indentation stress can then be calculated using the following two expressions:

$$\varepsilon = \frac{a}{R} \qquad (5)$$

$$\sigma = \frac{F}{\pi a^2} \qquad (6)$$

Indentation stress and strain are calculated for every cycle of the indentation, which finally produces a complete stress-strain curve that can be used to calculate a value of yield strength.

4 Results

4.1 Microstructural characterisation

EBSD showed that the average grain size did not significantly change after any of the heat treatments were performed, with the AR sample having an average grain diameter of 78 μm (excluding Σ3 twin boundaries) and no grain growth observed on the material aged at 700 °C. Therefore, all tests can be considered as being performed on single crystals since the deformed region will most likely be contained within a single grain.

Examples of Cr elemental maps obtained using STEM EDS, with background noise automatically removed within the acquisition software, can be seen in Figure 1. In the as-received material the Cr is in solution with the Cu matrix and no precipitates were observed. Some clusters of Cr became visible in the 400 °C sample but discrete precipitates were first clearly observed in the prime-aged material that had been heat treated at 480 °C. Larger and more defined precipitates were found in the 550 °C sample and this trend of increasing precipitate size with higher heat-treatment temperature is indicative of the other samples not shown here.

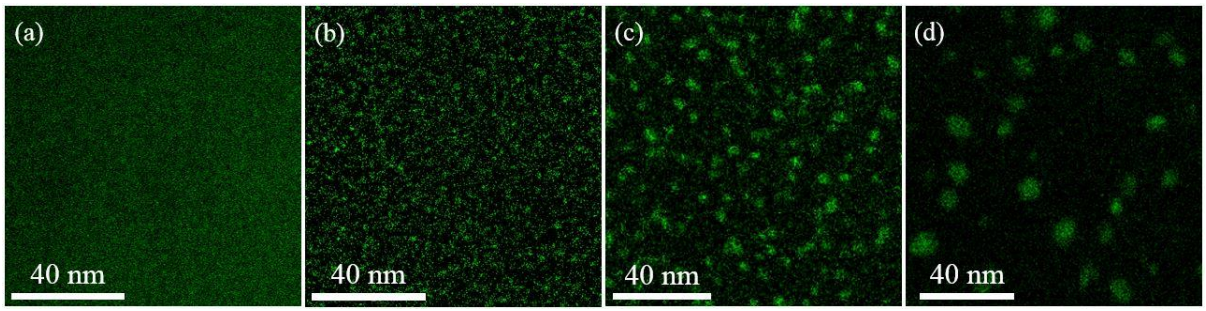

Figure 1: EDS chemical analysis Cr maps for (a) AR, (b) 400 °C, (c) 480 °C, and (d) 550 °C heat treated CuCrZr.

Table 1: Average precipitate diameter and spacings

Sample	Average precipitate diameter (nm)	Precipitate spacing (nm)
AR	Coherent in matrix	N/A
400	1.56	6.06
480	3.18	10.08
550	7.04	16.53

The results of Cr precipitate size and spacing using the EDX maps can be seen in

Table **1**. It should be noted that precipitate centre-to-centre spacing was calculated using an estimate of 110 nm for the sample thickness, since it was not possible at the time to measure the exact value. This was considered to be a reasonable approximation for the regions examined, based on the beam current used and signal intensity collected. Nevertheless, these measurements confirm that a variation in internal length-scale has been achieved via systematically heat-treating at different temperatures.

4.2 Spherical indentation

After failed or erroneous tests had been removed, linear interpolation was used to fit the raw data to equivalent a/R values and averaging was performed. A plot of indentation stress versus indentation strain for the AR material, all indenter tips, can be seen in Figure 2(a). As can be seen from the larger error bars, which here represent one standard deviation, data for the 2 μm tip was more scattered. This is likely due to the surface roughness having a larger impact on contact area miscalculation when penetration depths are smaller. The elastic modulus is also affected by this, which can be seen in Figure 2(b). The ISE is exhibited as higher hardness for smaller tip radii, however at high strains there is little variation between the responses from the largest four tips.

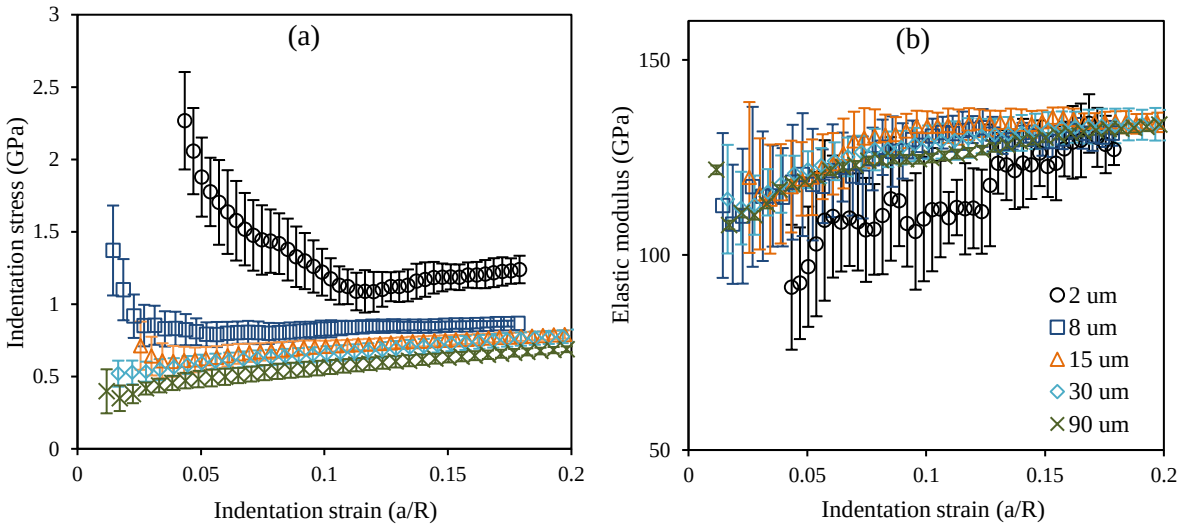

Figure 2: Indentation results for AR (solution annealed) CuCrZr using five indenters of different radii; (a) indentation stress and (b) elastic modulus as a function of indentation strain.

To calculate indentation yield pressure a linear fit to the plastic region of the averaged data was first made; this was then extrapolated back to the elastic line calculated from Hertzian mechanics (Eq. 2) and the yield pressure defined as the point of intersection. This approach has previously been used by Zhu et al. for ceramics [35] and metals [36]. This was carried out within a custom-made Python routine and an example of the final result for one sample and one indenter tip is shown in Figure 3.

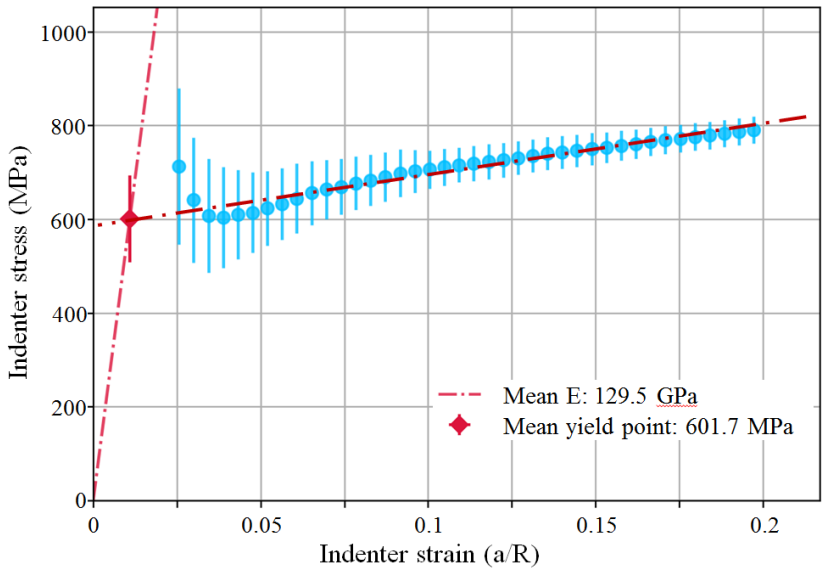

Figure 3: Example of method used to calculate indentation yield stress, here using the 15 µm tip on as-received CuCrZr.

In order to compare the response of the material at the initiation of plastic deformation and at more advanced stages, another measurement of pressure was made at 0.15Ɛ (or at a strain as close as possible to this value, if 0.15Ɛ was not achieved during indentation). The results from both these measurements, made on all samples with all indenter tips, can be seen in Figure **4**.

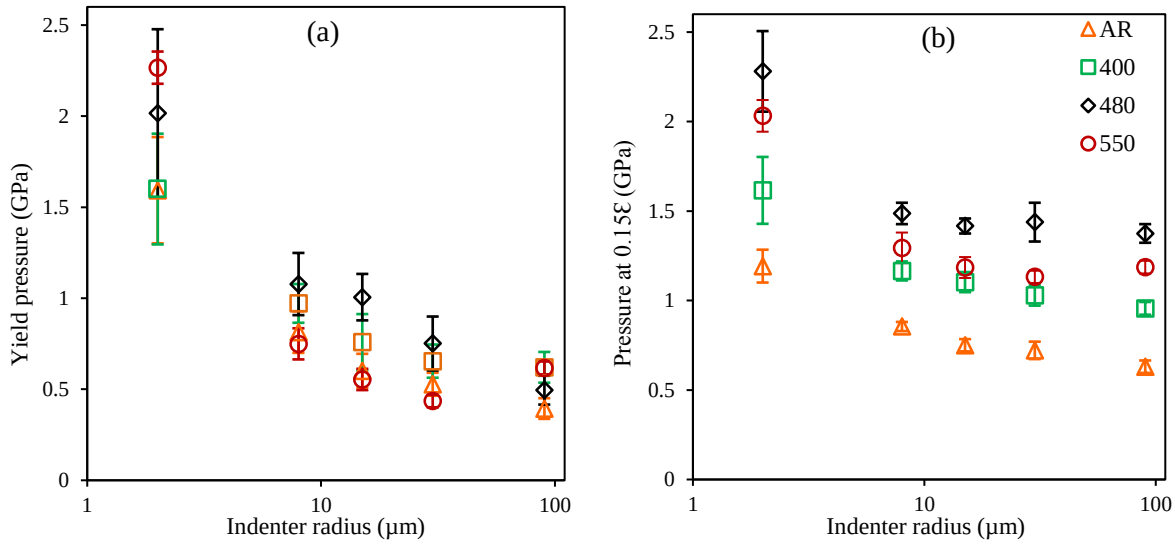

Figure 4: Hardness calculated at (a) intersect between elastic and extrapolated plastic lines, and (b) 0.15 indentation strain.

A pronounced ISE can be seen in Figure 4(a), showing a decrease in indentation yield pressure with an increase in indenter tip radius. There is not a great difference in hardness between the four samples, although as expected the material heat-treated at 480 °C exhibits the highest value at most indenter radii. A different result can be seen in Figure 4(b), however, where the ISE begins to taper off after an indenter radius of ~10 µm but a clear intrinsic size effect can be seen throughout.

5 Conclusions

By applying heat treatments to solution-annealed CuCrZr, a variation in precipitate size and spacing can be achieved that greatly alters the hardness of the material. When tested using spherical nanoindentation with different tip radii an ISE in hardness is clearly observed in all samples, as expected. What is interesting to note, however, is that the size effect due to test piece length-scale is less apparent in the later stages of plastic deformation. This would indicate that, past a certain point, dislocation-precipitate interaction is the dominant mechanism in resistance to plastic deformation in CuCrZr, meaning that outside of the elastic regime size-independent results can be obtained using spherical indenter tips in the range of ~tens µm. Similar results have been reported from TEM in-situ pillar compression of proton-irradiated Cu [37] and, more recently, in ion-irradiated Fe-9%Cr ODS alloy [38] where yield strengths similar to macroscopic values were recorded from irradiated pillars of ~ 400 nm and ~100 nm respectively. The authors of the former of these conclude that below this

value, “size-dependent strength results from dislocation source limitation”. Results from the investigation presented here support this idea, albeit at a larger test piece threshold due to the larger obstacle spacing, since a strong ISE can only be observed in the yield pressure, where smaller tips create a smaller plastic zone size and are therefore less likely to activate dislocation sources in a relatively dislocation-free material system.

Acknowledgements

This project has received funding from the EMPIR programme co-financed by the Participating States and from the European Union’s Horizon 2020 research and innovation. Equipment at the Materials Research Facility at UKAEA was used; the MRF is funded by the UK National Nuclear User Facility and Henry Royce Institute.

References

[1] A. Hernández-Pérez, M. Eddahbi, M.A. Monge, A. Munoz, B. Savoini, Microstructure and mechanical properties of an ITER-grade Cu-Cr-Zr alloy processed by equal channel angular pressing, Fusion Eng. Des. 98–99 (2015) 1978–1981. doi:10.1016/S1003-6326(11)60986-2.

[2] J.Y. Park, Y. Il Jung, B.-K. Choi, J.-S. Lee, Y.H. Jeong, B.G. Hong, Investigation on the microstructure and mechanical properties of CuCrZr after manufacturing thermal cycle for plasma facing component, J. Nucl. Mater. 417 (2011) 916–919. doi:10.1016/j.jnucmat.2010.12.157.

[3] M. Lipa, a. Durocher, R. Tivey, T. Huber, B. Schedler, J. Weigert, The use of copper alloy CuCrZr as a structural material for actively cooled plasma facing and in vessel components, Fusion Eng. Des. 75–79 (2005) 469–473. doi:10.1016/j.fusengdes.2005.06.056.

[4] ITER, Material Specification for the supply of CuCrZr - IG alloy seamless tubes for the ITER divertor, n.d.

[5] M.D. Uchic, P. a. Shade, D.M. Dimiduk, Plasticity of Micrometer-Scale Single Crystals in Compression, Annu. Rev. Mater. Res. 39 (2009) 361–386. doi:10.1146/annurev-matsci-082908-145422.

[6] E.M. Grieveson, D.E.J. Armstrong, S. Xu, S.G. Roberts, Compression of self-ion implanted iron micropillars, J. Nucl. Mater. (2012). doi:10.1016/j.jnucmat.2012.06.014.

[7] D.M. Dimiduk, M.D. Uchic, T.A. Parthasarathy, Size-affected single-slip behavior of pure nickel microcrystals, Acta Mater. 53 (2005) 4065–4077. doi:10.1016/j.actamat.2005.05.023.

[8] R. Fritz, D. Kiener, Development and application of a heated in-situ SEM micro-testing device, Meas. J. Int. Meas. Confed. 110 (2017) 356–366. doi:10.1016/j.measurement.2017.07.012.

[9] A.S. Schneider, D. Kiener, C.M. Yakacki, H.J. Maier, P.A. Gruber, N. Tamura, M. Kunz,

A.M. Minor, C.P. Frick, Influence of bulk pre-straining on the size effect in nickel compression pillars, Mater. Sci. Eng. A. 559 (2013) 147–158. doi:10.1016/j.msea.2012.08.055.

[10] C. Motz, T. Schöberl, R. Pippan, Mechanical properties of micro-sized copper bending beams machined by the focused ion beam technique, Acta Mater. 53 (2005) 4269–4279. doi:10.1016/j.actamat.2005.05.036.

[11] M.W. Kapp, T. Kremmer, C. Motz, B. Yang, R. Pippan, Structural instabilities during cyclic loading of ultrafine-grained copper studied with micro bending experiments, Acta Mater. 125 (2017) 351–358. doi:10.1016/j.actamat.2016.11.040.

[12] J. Ast, M. Göken, K. Durst, Size-dependent fracture toughness of tungsten, Acta Mater. 138 (2017) 198–211. doi:10.1016/j.actamat.2017.07.030.

[13] S.R. Jian, C.Y. Huang, W.C. Ke, Nanoindentation responses of InN thin films, J. Alloys Compd. 609 (2014) 125–128. doi:10.1016/j.jallcom.2014.04.128.

[14] A.E. Ozmetin, O. Sahin, E. Ongun, M. Kuru, Mechanical characterization of MgB2 thin films using nanoindentation technique, J. Alloys Compd. 619 (2015) 262–266. doi:10.1016/j.jallcom.2014.09.015.

[15] D.E.J. Armstrong, C.D. Hardie, J.S.K.L. Gibson, a. J. Bushby, P.D. Edmondson, S.G. Roberts, Small-scale characterisation of irradiated nuclear materials: Part II nanoindentation and micro-cantilever testing of ion irradiated nuclear materials, J. Nucl. Mater. 462 (2015) 374–381. doi:10.1016/j.jnucmat.2015.01.053.

[16] Y. Yee Lim, M M Chaudhri, The effect of the indenter load on the nanohardness of ductile metals: an experimental study on polycrystalline work-hardened and annealed oxygen-free copper, Philos. Mag. A. 79 (1999) 2979–3000. doi:10.1080/014186199251193.

[17] J. Swadener, The correlation of the indentation size effect measured with indenters of various shapes, J. Mech. Phys. Solids. 50 (2002) 681–694. doi:10.1016/S0022-5096(01)00103-X.

[18] A.J. Bushby, D.J. Dunstan, Plasticity size effects in nanoindentation, J. Mater. Res. 19 (2004) 137–142. doi:10.1557/jmr.2004.19.1.137.

[19] G.M. Pharr, E.G. Herbert, Y. Gao, The Indentation Size Effect: A Critical Examination of Experimental Observations and Mechanistic Interpretations, Annu. Rev. Mater. Res. 40 (2010) 271–292. doi:10.1146/annurev-matsci-070909-104456.

[20] E.O. Hall, Deformation and ageing of mild steel: {III} discussion of results, Proc. Phys. Soc. A. 64 (1951) 747–753.

[21] E.T. Lilleodden, W.D. Nix, Microstructural length-scale effects in the nanoindentation behavior of thin gold films, Acta Mater. 54 (2006) 1583–1593. doi:10.1016/j.actamat.2005.11.025.

[22] D.J. Dunstan, A.J. Bushby, Grain size dependence of the strength of metals: The Hall–Petch effect does not scale as the inverse square root of grain size, Int. J. Plast. 53 (2014) 56–65. doi:10.1016/j.ijplas.2013.07.004.

[23] N. a. Fleck, G.M. Muller, M.F. Ashby, J.W. Hutchinson, Strain gradient plasticity: Theory and experiment, Acta Metall. Mater. 42 (1994) 475–487. doi:10.1016/0956-7151(94)90502-9.

[24] W.D. Nix, H.J. Gao, Indentation size effects in crystalline materials: A law for strain gradient plasticity, J. Mech. Phys. Solids. 46 (1998) 411–425. doi:10.1016/s0022-5096(97)00086-0.

[25] J.R. Greer, W.C. Oliver, W.D. Nix, Size dependence of mechanical properties of gold at the micron scale in the absence of strain gradients, Acta Mater. 53 (2005) 1821–1830. doi:10.1016/j.actamat.2004.12.031.

[26] T.T. Zhu, A.J. Bushby, D.J. Dunstan, Materials mechanical size effects: a review, Mater. Technol. 23 (2008) 193–209. doi:10.1179/175355508X376843.

[27] O. Kraft, P. a. Gruber, R. Mönig, D. Weygand, Plasticity in Confined Dimensions, Annu. Rev. Mater. Res. 40 (2010) 293–317. doi:10.1146/annurev-matsci-082908-145409.

[28] D.J. Dunstan, A.J. Bushby, The scaling exponent in the size effect of small scale plastic deformation, Int. J. Plast. 40 (2013) 152–162. doi:10.1016/j.ijplas.2012.08.002.

[29] D.J. Edwards, B.N. Singh, S. Tähtinen, Effect of heat treatments on precipitate microstructure and mechanical properties of a CuCrZr alloy, J. Nucl. Mater. 367–370 B (2007) 904–909. doi:10.1016/j.jnucmat.2007.03.064.

[30] A. Chbihi, X. Sauvage, D. Blavette, Atomic scale investigation of Cr precipitation in copper, Acta Mater. 60 (2012) 4575–4585. doi:10.1016/j.actamat.2012.01.038.

[31] A.J. Bushby, N.M. Jennett, Determining the Area Function of Spherical Indenters for Nanoindentation., MRS Proc. 649 (2011) Q7.17. doi:10.1557/PROC-649-Q7.17.

[32] J.S. Field, M. V Swain, A simple predictive model for spherical indentation, J. Mater. Res. 8 (1993) 297–306. doi:10.1557/JMR.1993.0297.

[33] J. Schindelin, I. Arganda-Carreras, E. Frise, V. Kaynig, M. Longair, T. Pietzsch, S. Preibisch, C. Rueden, S. Saalfeld, B. Schmid, J.-Y. Tinevez, D.J. White, V. Hartenstein, K. Eliceiri, P. Tomancak, A. Cardona, Fiji: an open-source platform for biological-image analysis, Nat Meth. 9 (2012) 676–682. http://dx.doi.org/10.1038/nmeth.2019.

[34] H. Hertz, On the contact of rigid elastic solids and on hardness, (n.d.).

[35] T.T. Zhu, A.J. Bushby, D.J. Dunstan, Size effect in the initiation of plasticity for ceramics in nanoindentation, J. Mech. Phys. Solids. 56 (2008) 1170–1185. doi:10.1016/j.jmps.2007.10.003.

[36] T.T. Zhu, X.D. Hou, A.J. Bushby, D.J. Dunstan, Size effect at the initiation of plasticity for ceramics and metals, J. Appl. Phys. D Appl. Phys. 41 (2008). doi:10.1088/0022-3727/41/7/074004.

[37] D. Kiener, P. Hosemann, S.A. Maloy, A.M. Minor, In situ nanocompression testing of irradiated copper, Nat. Mater. 10 (2011) 608–613. doi:10.1038/nmat3055.

[38] K.H. Yano, M.J. Swenson, Y. Wu, J.P. Wharry, TEM in situ micropillar compression tests of ion irradiated oxide dispersion strengthened alloy, J. Nucl. Mater. 483 (2017) 107–120. doi:10.1016/j.jnucmat.2016.10.049.